Polyhedron 208 (2021) 115445

Contents lists available at ScienceDirect

Polyhedron

journal homepage: www.elsevier.com/locate/poly

Coordination networks assembled from $Co(NCS)_2$ and 4′-[4-(naphthalen-1-yl)phenyl]-3,2′:6′,3″-terpyridine: Role of lattice solvents

Dalila Rocco, Samantha Novak, Alessandro Prescimone, Edwin C. Constable, Catherine E. Housecroft *

Department of Chemistry, University of Basel, Mattenstrasse 24a, BPR 1096, 4058 Basel, Switzerland

ARTICLE INFO

Dedication: We dedicate this manuscript to the memory of Malcolm L. H. Green. ECC particularly wishes to acknowledge the influence that Malcolm's inspiring and enthusiastic teaching had in catalyzing ECC's transformation from an organic to an inorganic chemist.

Keywords:
3,2′:6′,3″-Terpyridine
Cobalt
Lattice solvent
Coordination networks

ABSTRACT

The preparation and characterization of 4′-[4-(naphthalen-1-yl)phenyl]-3,2′:6′,3″-terpyridine (**1**) are described. Reactions of **1** with $Co(NCS)_2$ under conditions of crystal growth by layering using different solvent combinations produced crystals of $[Co(\mathbf{1})_2(NCS)_2]_n{\cdot}2n CHCl_3$ and $[Co(\mathbf{1})_2(NCS)_2]_n{\cdot}2n C_6H_5Me$, each of which comprised a (4,4) net. The orientations of **1** with respect to the planar network defined by the Co atoms are significantly different in $[Co(\mathbf{1})_2(NCS)_2]_n{\cdot}2n C_6H_5Me$ compared to $[Co(\mathbf{1})_2(NCS)_2]_n{\cdot}2n CHCl_3$, and the toluene molecules in $[Co(\mathbf{1})_2(NCS)_2]_n{\cdot}2n C_6H_5Me$ are involved in π-stacking interactions. The solvent-accessible void-space in the latter consists of a series of interlinked cavities in contrast to the open channels in $[Co(\mathbf{1})_2(NCS)_2]_n{\cdot}2n CHCl_3$. Thermogravimetric analysis was used to investigate solvent loss and uptake in the two coordination networks. After solvent loss from $[Co(\mathbf{1})_2(NCS)_2]_n{\cdot}2n CHCl_3$, $CHCl_3$, $CDCl_3$ or CH_2Cl_2 could be taken up by the lattice. In contrast, removal of toluene from $[Co(\mathbf{1})_2(NCS)_2]_n{\cdot}2n C_6H_5Me$ was found to be irreversible.

1. Introduction

While less well developed than that of 2,2′:6′,2″-terpyridine (tpy) [1–5], the coordination chemistry of 3,2′:6′,3″-terpyridine (3,2′:6′,3″-tpy) has gained increased attention over the last decade, especially in the context of coordination polymers and networks [6–9]. The 3,2′:6′,3″-tpy metal-binding domain is conformationally flexible, and Scheme 1 displays its three limiting, planar conformations. Different conformations can be observed in the solid-state structures of 3,2′:6′,3″-tpy ligands depending upon the 4′-substituents, both in the free ligands [10] and in coordination polymers [11–13]. Conformations **A** and **B** (Scheme 1) can be classified as divergent and are to be the expected limiting conformations favoured when 3,2′:6′,3″-tpy ligands are incorporated as linkers in coordination polymers. In contrast, conformation **C** can participate in the assembly of small discrete multinuclear complexes [12,14], in addition to coordination polymers. Note that the central pyridine ring remains uncoordinated in all cases.

Combinations of $Co(NCS)_2$ and 4′-functionalized 3,2′:6′,3″-tpy ligands typically lead to (4,4) networks with each Co(II) centre bound by *trans*-thiocyanato ligands and four pyridine *N*-donors of four different 3,2′:6′,3″-tpy ligands [10,15,16]. Similarly, reactions of $Co(NCS)_2$ and 4′-functionalized 4,2′:6′,4″-tpy ligands also usually produce 2-dimensional (4,4) nets [17–22], although the unexpected assembly of 3-dimensional architectures has been observed in a few cases [20,23]. Where crystals have been grown by layering a MeOH solution of $Co(NCS)_2$ under ambient conditions, the dominant product may be a 1-dimensional polymer $[Co(NCS)_2(MeOH)_2(L)]_n$ (L = 4′-functionalized 3,2′:6′,3″-tpy or 4,2′:6′,4″-tpy) [15,19,21].

We have previously carried out systematic investigations of the effects of different 4′-substituents R on the assembly of $[Co(NCS)_2(4'\text{-}R\text{-}3,2':6',3''\text{-tpy})_2]_n$ 2-dimensional nets [10,15,16], and have demonstrated a change between conformations **A** and **B** (Scheme 1) as a consequence of changing the 4′-substituent. Motivated by these results and the observation that many of the 2D structures contain lattice solvent molecules, we decided to focus on a single 3,2′:6′,3″-tpy ligand (**1**, Scheme 2) and explore the effects of using different pairs of solvents in crystal growth experiments. Here we report the coordination networks assembled when MeOH or MeCN solutions of $Co(NCS)_2$ were layered

* Corresponding author.
E-mail address: catherine.housecroft@unibas.ch (C.E. Housecroft).

https://doi.org/10.1016/j.poly.2021.115445
Received 5 July 2021; Accepted 17 August 2021
Available online 24 August 2021

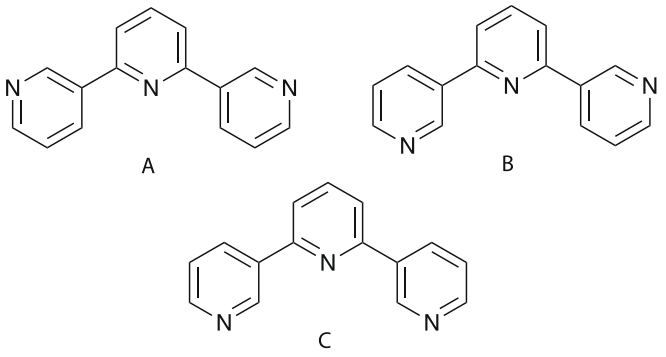

Scheme 1. Limiting planar conformations of 3,2′:6′,3″-tpy.

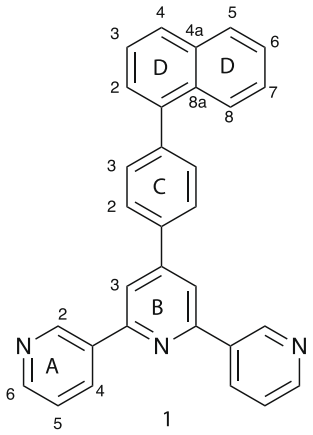

Scheme 2. Structure of compound **1** and numbering for NMR spectroscopic assignments.

over toluene or $CHCl_3$ solutions of **1**. Ligand **1** was selected because of the potential for π-stacking interactions involving the extended aromatic system [24,25] and the possibility of using the supramolecular effects to further control and refine the structure.

2. Materials and methods

2.1. General

^1H, $^{13}C\{^1H\}$ and 2D NMR spectra were recorded on a Bruker Avance III-500 spectrometer equipped with a BBFO probehead at 298 K. The ^1H and ^{13}C NMR chemical shifts were referenced with respect to residual solvent peaks (δ TMS = 0). A Shimadzu LCMS-2020 instrument was used to record electrospray ionization (ESI) mass spectra, and FT-infrared (IR) spectra were recorded on a PerkinElmer UATR Two instrument. A Shimadzu UV2600 spectrophotometer was used to record solution absorption spectra.

Thermogravimetric analysis (TGA) was performed on a TGA5500 instrument (TA Instruments) coupled to a Discovery II MS, Cirrus 3, Mass Spectrometer, DMS. The analysis was carried under nitrogen, using a Barchart scanning method in the mass range 10–125. In all the experiments, the temperature of the TGA instrument was initially stabilized at 30 °C. The samples were then heated to the appropriate temperature, depending upon the solvent included in the lattice and this temperature was maintained for 10–30 min. During this time, it was possible to detect the solvent being released from the coordination network (see Section 3.4 for details) and solvents were identified through mass spectrometry. Afterwards the samples were cooled to ambient temperature and put in contact with vapors of the same or a different solvent for 24–72 h, After this, the TGA was repeated using the same procedure. A set of measurements was performed on each coordination network.

3-Acetylpyridine was purchased from Acros Organics, 4-(naphthalen-1-yl)benzaldehyde from Fluorochem and cobalt(II) thiocyanate from Sigma Aldrich. All chemicals were used as received.

All crystal growth experiments were carried out under ambient conditions using identical glass crystallization tubes (i.d. = 13.6 mm, 24 mL).

2.2. Compound *1*

4-(Naphthalen-1-yl)benzaldehyde (1.00 g, 4.31 mmol) was dissolved in EtOH (50 mL) and then 3-acetylpyridine (1.04 g, 0.95 mL, 8.62 mmol) and crushed KOH (0.484 g, 8.62 mmol) were added to the solution. An excess of aqueous NH_3 (32%, 16.6 mL) was slowly added to the reaction mixture which was then stirred at room temperature (ca. 22 °C) overnight. The solid that formed was collected by filtration, washed with H_2O (3 × 10 mL) and EtOH (3 × 10 mL), recrystallized from EtOH and dried in vacuo. Compound **1** was isolated as a colorless solid (0.789 g, 1.81 mmol, 42.0%). M.p. = 225 °C. ^1H NMR (500 MHz, $CDCl_3$): δ/ppm 9.46 (dd, J = 2.3, 0.9 Hz, 2H, H^{A2}), 8.75 (dd, J = 4.9, 1.6 Hz, 2H, H^{A6}), 8.68 (dt, J = 8.0, 2.0 Hz, 2H, H^{A4}), 8.11 (s, 2H, H^{B3}), 7.94 (overlapping m, 5H, H^{C2} + $3H^{D}$), 7.72 (m, 2H, H^{C3}), 7.62–7.47 (overlapping m, 6H, H^{A5} + $4H^{D}$). $^{13}C\{^1H\}$ NMR (126 MHz, $CDCl_3$): δ/ppm 155.0 (C^{A3}), 151.2 (C^{B4}), 148.8 (C^{A6}), 147.1 (C^{A2}), 142.6 (C^{C4}), 139.2 (C^{D1}), 136.8 (C^{C1}), 136.1 (C^{A4}), 135.4 (C^{B2}), 134.0 ($C^{D4a/D8a}$), 131.6 ($C^{D4a/D8a}$), 131.3 (C^{C3}), 128.6 (C^{D}), 128.4 (C^{D}), 127.3 (C^{C2}), 127.2 (C^{D}), 126.5 (C^{D}), 126.1 (C^{D}), 125.8 (C^{D}), 125.6 (C^{D}), 124.4 (C^{A5}), 118.3 (C^{B3}). UV–VIS (MeCN, 2.0 × 10^{-5} mol dm^{-3}) λ/nm 222 (ε/dm^3 mol^{-1} cm^{-1} 62,600), 258 (35,500), 294 (25,900). ESI-MS m/z 436.17 $[M+H]^+$ (calc. 436.18). Found C 85.51, H 4.81, N 9.79; required for $C_{31}H_{21}N_3$ C 85.49, H 4.86, N 9.65.

2.3. *[Co(1)$_2$(NCS)$_2$]$_n$·2nCHCl$_3$*

A solution of $Co(NCS)_2$ (5.3 mg, 0.030 mmol) in MeCN (6 mL) was layered over a $CHCl_3$ solution (5 mL) of **1** (13.1 mg, 0.030 mmol). Pink block-like crystals grew after 10 days. A single crystal was selected for X-ray diffraction and the remaining crystals were washed with MeCN and $CHCl_3$, dried under vacuum and analysed by PXRD and FT-IR spectroscopy.

2.4. *[Co(1)$_2$(NCS)$_2$]$_n$·2nC$_6$H$_5$Me*

A solution of $Co(NCS)_2$ (5.3 mg, 0.030 mmol) in MeOH (6 mL) was layered over a toluene solution (6 mL) of **1** (13.1 mg, 0.030 mmol). Pink plate-like crystals grew after 7 days. A single crystal was selected for X-ray diffraction and the remaining crystals were washed with MeOH and toluene, dried under vacuum and analysed by PXRD and FT-IR spectroscopy.

2.5. Crystallography

Single crystal data were collected on a Bruker APEX-II diffractometer (CuKα radiation) with data reduction, solution and refinement using the programs APEX [26], ShelXT [27], Olex2 [28] and ShelXL v. 2014/7 [29]. All H atoms were included at geometrically calculated positions and refined using a riding model with U_{iso} = 1.2 of the parent atom. Structure analysis and structural diagrams used CSD Mercury 2020.1 [30]. In $[Co(\mathbf{1})_2(NCS)_2]_n\cdot 2nC_6H_5Me$, each toluene solvent molecule was disordered over a symmetry element, with site occupancies of 50%; the toluene molecules were refined isotropically. In $[Co(\mathbf{1})_2(NCS)_2]_n\cdot 2nCHCl_3$, the solvent area was treated using a solvent mask, and the electron density removed corresponded to 2 molecules of $CHCl_3$ per Co atom; this was added to the formulae and appropriate numbers.

PXRD patterns were collected at ca. 298 K in transmission mode

using a Stoe Stadi P diffractometer with Cu Kα1 radiation (Ge(111) monochromator) and a DECTRIS MYTHEN 1 K detector. Whole-pattern decomposition (profile matching) analysis [31–33] of the diffraction patterns was performed with the package FULLPROF SUITE [33,34] (v. September 2020) using a previously determined instrument resolution function based on a NIST640d standard. The structural models were taken from the single crystal X-Ray diffraction refinements. Refined parameters in Rietveld were: scale factor, zero shift, lattice parameters, Co and S atomic positions, background points and peaks shapes as a Thompson-Cox-Hastings pseudo-Voigt function. Preferred orientations were included in the analysis as a March-Dollase multi-axial phenomenological model.

2.6. $[Co(\mathbf{1})_2(NCS)_2]_n{\cdot}2nCHCl_3$

$C_{66}H_{44}Cl_6CoN_8S_2$, M_r = 1284.919, pink block, monoclinic, space group $P2_1/n$, a = 10.9048(6), b = 18.5289(10), c = 15.4837(8) Å, β = 91.214(3)°, V = 3127.8(3) Å^3, D_c = 1.364 g cm^{-3}, T = 150 K, Z = 2, μ(CuKα) = 5.508 mm^{-1}. Total 18,857 reflections, 5644 unique (R_{int} = 0.0327). Refinement of 5210 reflections (340 parameters) with $I > 2\sigma(I)$ converged at final R_1 = 0.0442 (R_1 all data = 0.0474), wR_2 = 0.1226 (w$R2$ all data = 0.1261), gof = 1.0431. CCDC 2087183.

2.7. $[Co(\mathbf{1})_2(NCS)_2]_n{\cdot}2nC_6H_5Me$

$C_{78}H_{58}CoN_8S_2$, M_r = 1230.37, pink plate, monoclinic, space group $P2_1/c$, a = 14.6063(5), b = 11.8567(5), c = 18.3485(6) Å, β = 92.912(2)°, V = 3173.5(2) Å^3, D_c = 1.288 g cm^{-3}, T = 150 K, Z = 2, μ(CuKα) = 3.137 mm^{-1}. Total 20,072 reflections, 5706 unique (R_{int} = 0.0368). Refinement of 5130 reflections (375 parameters) with $I > 2\sigma(I)$ converged at final R_1 = 0.0583 (R_1 all data = 0.0646), wR_2 = 0.1557 (w$R2$ all data = 0.1612), gof = 1.050. CCDC 2087184.

3. Results and discussion

3.1. Ligand synthesis and characterization

Compound **1** was prepared by the one-pot strategy of Wang and Hanan [35] by reaction of two equivalents of 3-acetylpyridine with 4-(naphthalen-1-yl)benzaldehyde under basic conditions and addition of aqueous NH_3. The ligand was isolated in 42.0% yield as a colorless solid, and the base peak in the ESI mass spectrum corresponded to the $[M+H]^+$ ion (m/z 436.17, Fig. S1). The ^{1}H and ^{13}C{^{1}H} NMR spectra (Figs. S2 and S3, respectively) were assigned using NOESY, COSY, HMQC (Fig. S4) and HMBC (Fig. S5) spectra, and were in accord with the structure shown in Scheme 2. Overlap of the signals for the naphthyl protons made unambiguous assignment of these signals difficult. The IR spectrum is shown in Fig. S6, with diagnostic, strong bands in the fingerprint region at 796, 773 and 695 cm^{-1}. Fig. 1 displays the solution absorption spectrum of **1**, and the absorption bands are assigned to π*←π transitions. The spectrum closely resembles that of 4′-[4-(naphthalen-1-yl)phenyl]-4,2′:6′,4″-terpyridine [36] which is an isomer of **1**.

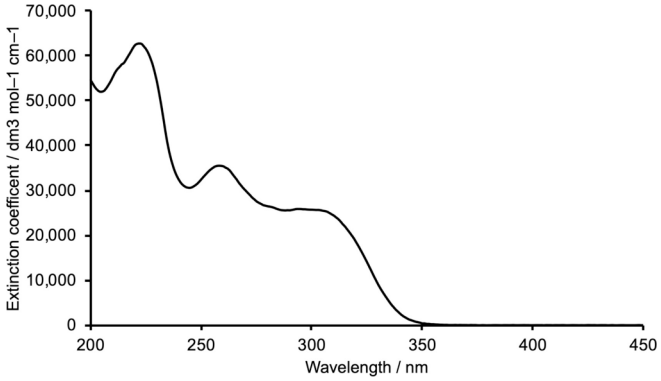

Fig. 1. The absorption spectrum of **1** (MeCN, 2.0 × 10^{-5} mol dm^{-3}).

3.2. Coordination networks $[Co(\mathbf{1})_2(NCS)_2]_n{\cdot}2nCHCl_3$ and $[Co(\mathbf{1})_2(NCS)_2]_n{\cdot}2nC_6H_5Me$

Single crystals of $[Co(\mathbf{1})_2(NCS)_2]_n{\cdot}2nCHCl_3$ and $[Co(\mathbf{1})_2(NCS)_2]_n{\cdot}2nC_6H_5Me$ were grown under ambient conditions by layering either a MeCN solution of $Co(NCS)_2$ over a $CHCl_3$ solution of **1**, or a MeOH solution of $Co(NCS)_2$ over a toluene solution of **1**, respectively. X-ray quality crystals were selected and the remaining crystals were used for PXRD analysis (see Section 3.3). The two compounds crystallize in the monoclinic space groups $P2_1/n$ and $P2_1/c$, respectively, and each possesses a 2D-network with the Co(II) centers acting as 4-connecting nodes. The structures of the asymmetric units with symmetry-generated atoms are shown in Fig. 2. The Co atom in each structure is six-coordinate and lies on an inversion center, being bonded to four different, but crystallographically equivalent, ligands **1**. Selected bond lengths and angles in each cobalt(II) coordination sphere are given in Table 1 and are unexceptional.

In $[Co(\mathbf{1})_2(NCS)_2]_n{\cdot}2nCHCl_3$, **1** adopts conformation **A** in Scheme 1, whereas in $[Co(\mathbf{1})_2(NCS)_2]_n{\cdot}2nC_6H_5Me$, conformation **B** (Scheme 1) is observed. This results in distinct differences between the 2D-assemblies in $[Co(\mathbf{1})_2(NCS)_2]_n{\cdot}2nC_6H_5Me$ and $[Co(\mathbf{1})_2(NCS)_2]_n{\cdot}2nCHCl_3$. This is quantified by a comparison of the angles between the planes of adjacent aromatic rings in the ligand in each structure presented in Table 2. When **1** adopts conformation **A** (Scheme 1), the vectorial properties of each N1 and N3 in each ligand are equivalent. In contrast, the different vectorial properties of the *N*-donor lone pairs when ligand **1** is in conformation **B** lead to three possible coordination modes for a *trans*-arrangement of ligands. In a previous publication, we defined the labels *in* and *out* to describe the orientation of each N lone pair with respect to the central pyridine ring (Scheme 3) [13]. Since the Co atom in $[Co(\mathbf{1})_2(NCS)_2]_n{\cdot}2nC_6H_5Me$ lies on a center of symmetry, only two of the three coordination modes shown in Scheme 3 are permitted. Since each Co in $[Co(\mathbf{1})_2(NCS)_2]_n{\cdot}2nC_6H_5Me$ is crystallographically equivalent, both *trans out/out* and *in/in* arrangements are present at each metal center (Fig. 3a). This contrasts with the arrangement in $[Co(\mathbf{1})_2(NCS)_2]_n{\cdot}2nCHCl_3$ in which all motifs are *out/out* (Fig. 3b), leading to a significant difference between the $\{Co(\mathbf{1})_4\}$ units in the networks (Fig. 3a versus 3b).

Part of the (4,4) network in $[Co(\mathbf{1})_2(NCS)_2]_n{\cdot}2nCHCl_3$ is shown in Fig. 4a. The Co atoms are coplanar, and the 4-(naphthalen-1-yl)phenyl substituents protrude above and below the plane defined by the Co atoms. Around each rhombus in the net, the 4-(naphthalen-1-yl)phenyl groups are arranged in an *up/up/down/down* configuration (Fig. S7), and adjacent 2D-sheets are locked together by face-to-face π-stacking interactions between naphthalenyl rings in one layer with the central pyridine ring of the 3,2′:6′,3″-tpy units in the neighboring sheet (Fig. 4c). Metrics for the π-π interaction are centroid…centroid = 3.60 Å, and angle between the ring planes = 3.1°. The *up/up/down/down* configuration of the arene substituents leads to extended π-stacking interactions which interconnect all adjacent sheets in the lattice. Viewing the structure of $[Co(\mathbf{1})_2(NCS)_2]_n{\cdot}2nCHCl_3$ down the *a*-axis without solvent molecules present reveals approximately linear channels (Fig. 4d) and the solvent accessible void space in the lattice is ca. 25% of the total volume.

In $[Co(\mathbf{1})_2(NCS)_2]_n{\cdot}2nC_6H_5Me$, each toluene molecule is disordered over a symmetry element, with 50% site occupancies of head-to-tail positions. For the discussion below, one position for each toluene molecule is considered. Two views of the (4,4) net in $[Co(\mathbf{1})_2(NCS)_2]_n{\cdot}2nC_6H_5Me$ are depicted in Fig. 5a and 5b. As in $[Co(\mathbf{1})_2(NCS)_2]_n{\cdot}2nCHCl_3$ (Fig. 4), the Co atoms in each sheet are coplanar, and the terpyridines adopt an *up/up/down/down* arrangement around each rhombus (Fig. 5c). Inspection of Fig. 5a and 5c reveals that ligands **1** lie over the rhombuses in the net in

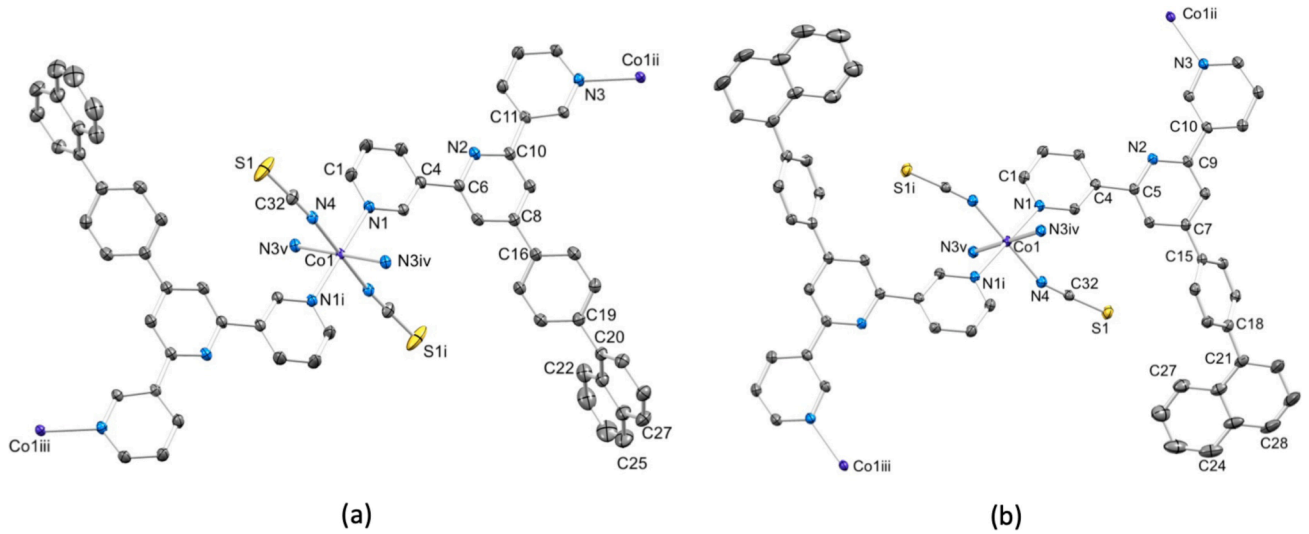

Fig. 2. The structures of the asymmetric units with symmetry-generated atoms in (a) $[Co(\mathbf{1})_2(NCS)_2]_n{\cdot}2n CHCl_3$ (symmetry codes: i = $-x$, $1-y$, $1-z$; ii = $^1/_2-x$, $-^1/_2+y$, $^1/_2-z$; iii = $-^1/_2-x$, $^1/_2+y$, $^3/_2-z$; iv = $^1/_2-x$, $^1/_2+y$, $^1/_2-z$; v = $-^1/_2+x$, $^1/_2-y$, $^1/_2+z$), and (b) $[Co(\mathbf{1})_2(NCS)_2]_n{\cdot}2n C_6H_5Me$ (symmetry codes: i = $1-x$, $1-y$, $-z$; ii = $1-x$, $^1/_2+y$, $^1/_2-z$; iii = $1-x$, $-^1/_2+y$, $-^1/_2-z$; iv = x, $^3/_2-y$, $-^1/_2+z$; v = $1-x$, $-^1/_2+y$; $^1/_2-z$). Ellipsoids are plotted at a 40% probability level, and H atoms and solvent molecules are omitted.

Table 1
Selected bond lengths and angles in $[Co(\mathbf{1})_2(NCS)_2]_n{\cdot}2n CHCl_3$, and $[Co(\mathbf{1})_2(NCS)_2]_n{\cdot}2n C_6H_5Me$.

Compound	Co–N_{NCS}/Å	Co–N_{py}/Å	N_{py}–Co–N_{NCS}/°	N_{py}–Co–N_{py}/°
$[Co(\mathbf{1})_2(NCS)_2]_n{\cdot}2n CHCl_3$	2.0769(16)	2.1886(16), 2.2241(16)	90.30(6), 89.70(6), 92.25(6), 87.75(6)	88.19(6), 91.81(6)
$[Co(\mathbf{1})_2(NCS)_2]_n{\cdot}2n C_6H_5Me$	2.084(2)	2.190(2), 2.239(2)	88.26(9), 91.74(9), 87.97(9), 92.03(9)	89.60(9), 90.40(9)

Table 2
Angles between planes of adjacent aromatic rings in $[Co(\mathbf{1})_2(NCS)_2]_n{\cdot}2n CHCl_3$, and $[Co(\mathbf{1})_2(NCS)_2]_n{\cdot}2n C_6H_5Me$.

Compound	py_{N1}/py_{N2}/°	py_{N2}/py_{N3}/°	py_{N2}/C_6H_4/°	C_6H_4/naphthyl/°
$[Co(\mathbf{1})_2(NCS)_2]_n{\cdot}2n CHCl_3$	15.8	15.6	34.8	53.6
$[Co(\mathbf{1})_2(NCS)_2]_n{\cdot}2n C_6H_5Me$	33.2	22.4	50.5	64.3

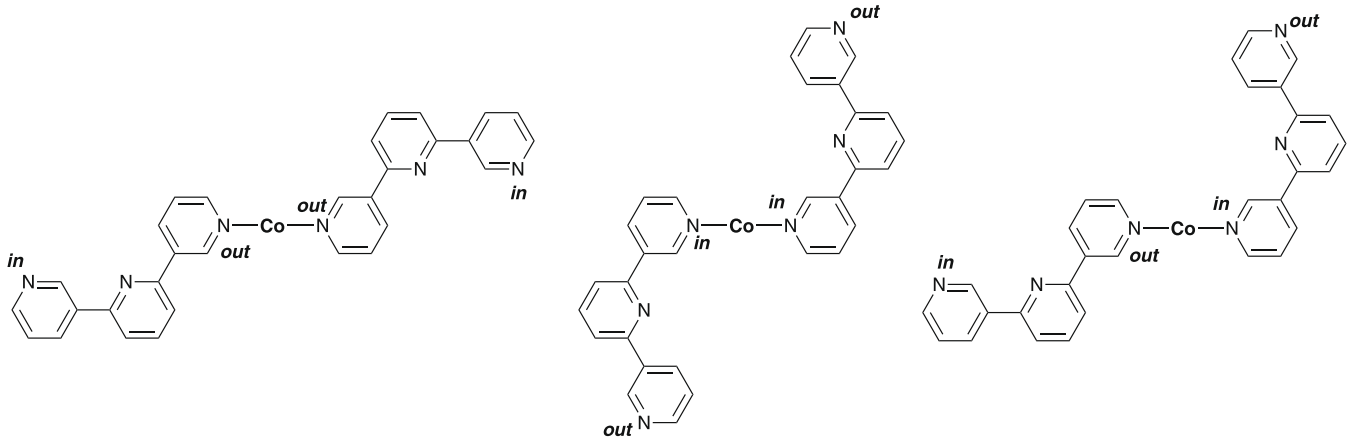

Scheme 3. Three coordination modes are possible for a *trans*-arrangement of ligands at a Co center, but only the left-hand two modes are permitted when the metal ion lies at a center-of-symmetry.

$[Co(\mathbf{1})_2(NCS)_2]_n{\cdot}2n C_6H_5Me$, in contrast to the upright positions found in $[Co(\mathbf{1})_2(NCS)_2]_n{\cdot}2n CHCl_3$ (Figs. 4a and S7). This impacts on the solvent accessible voids in the lattice (Fig. 5d and S8) which comprise a series of interlinked cavities (ca. 24% of the total lattice volume) in contrast to the open channels in $[Co(\mathbf{1})_2(NCS)_2]_n{\cdot}2n CHCl_3$. The toluene molecules occupying the cavities are involved in a face-to-face π-interaction with the pyridine ring containing N2, and C–H_{py}…$\pi_{toluene}$ contacts involving the pyridine rings with N2 and N3 (Fig. S10). For the face-to-face contact, the distance between the ring centroids is 3.8 Å and the angle between the ring planes is 9.8°. For the C–H_{py}…$\pi_{toluene}$ contacts, the H…centroid distances are 3.2 and 3.4 Å, and the C—H…centroid angles are 151 and 168°, respectively.

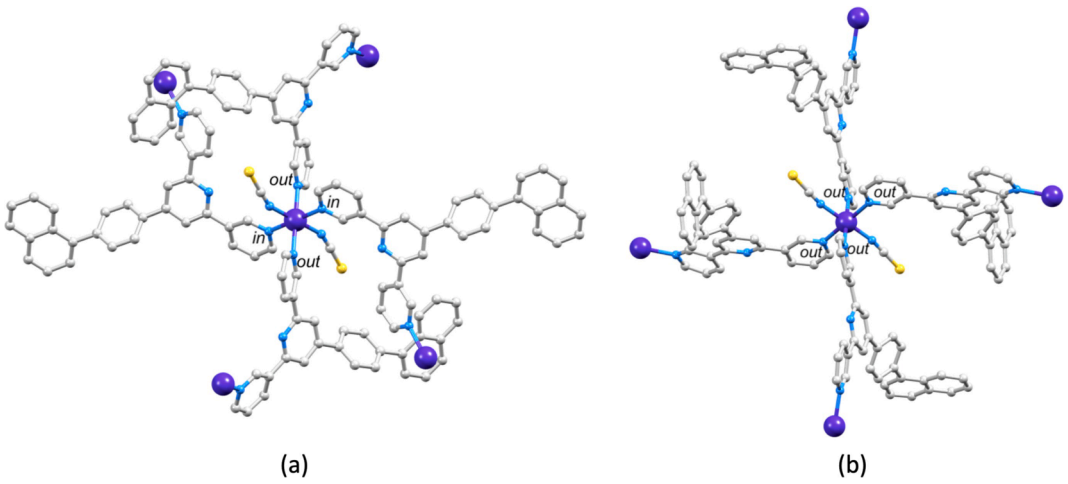

Fig. 3. The arrangement of ligands **1** in the coordination sphere of the Co atom in (a) $[Co(\mathbf{1})_2(NCS)_2]_n \cdot 2n C_6H_5Me$, and (b) $[Co(\mathbf{1})_2(NCS)_2]_n \cdot 2n CHCl_3$. See Scheme 3 for definitions of the *in* and *out* labels.

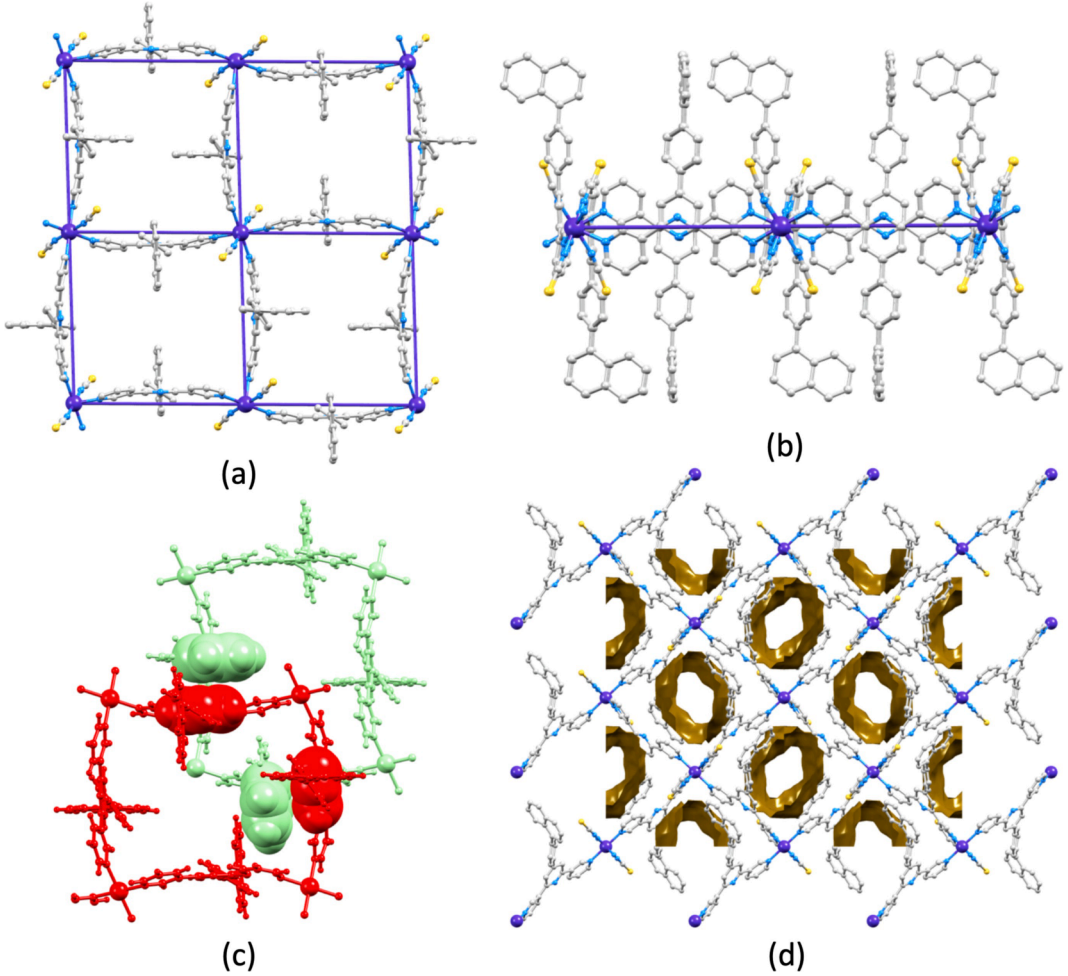

Fig. 4. The structure of $[Co(\mathbf{1})_2(NCS)_2]_n \cdot 2n CHCl_3$. (a) Part of one (4,4) net with connection lines between the Co atoms to emphasize the network topology; H atoms and solvent molecules are omitted for clarity. (b) The network viewed from the side to illustrate the positions of the peripheral naphthalenyl groups. (c) Stacking of naphthalenyl and 3,2′:6′,3″-domains in adjacent 2D-sheets. (d) View down the *a*-axis (solvent molecules omitted) showing the void (calculated using a contact surface map with probe radius = 1.2 Å); drawn using Mercury 2020.1 [30].

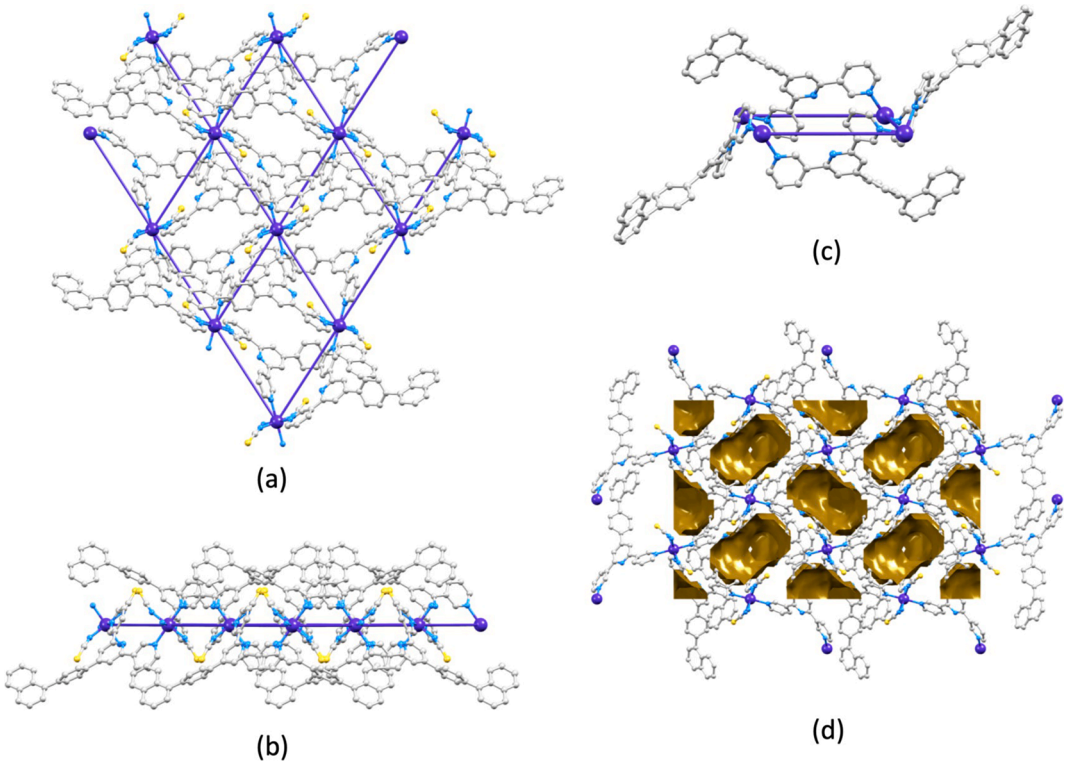

Fig. 5. The structure of $[Co(\mathbf{1})_2(NCS)_2]_n{\cdot}2n C_6H_5Me$. (a) Part of one 2D-net with connection lines between the Co atoms to highlight the (4,4) net; H atoms and solvent molecules are omitted for clarity, and (b) the same portion of the net viewed into the plane containing the Co atoms. (c) Arrangement of ligands **1** around a rhombus in the net. (d) View down the *a*-axis (solvent molecules omitted) showing the void space; drawn using Mercury 2020.1, and calculated using a contact surface map with a probe radius of 1.2 Å [30].

3.3. Analysis of bulk samples of the single crystals

In order to verify that the crystals selected for single-crystal X-ray diffraction were representative of the bulk crystalline materials, we carried out PXRD on the remaining crystals in each crystallization tube (see Sections 2.3 and 2.4). Fig. 6 shows comparisons of the experimental PXRD patterns (in red in Fig. 6) and the patterns predicted from the single crystal structures (in black in Fig. 6). For each compound, there was a match for every peak in the predicted pattern with those in the experimental PXRD pattern. No additional peaks were observed in the PXRD of the bulk materials.

The IR spectra of the cobalt(II) compounds are shown in Figs. S10 and S11. Bands in the fingerprint region are mainly characteristic of coordinated **1**. The dominant absorption at 2063 cm^{-1} for $[Co(\mathbf{1})_2(NCS)_2]_n{\cdot}2nCHCl_3$, and 2070 cm^{-1} for $[Co(\mathbf{1})_2(NCS)_2]_n{\cdot}2nC_6H_5Me$ arises from the CN stretching mode of the thiocyanato ligands.

3.4. Thermogravimetric analysis: Solvent removal and re-entry

Crystals of $[Co(\mathbf{1})_2(NCS)_2]_n{\cdot}2nCHCl_3$ were heated to 80 °C in the TGA instrument, and this temperature was maintained for 10 min. Loss of $CHCl_3$ was detected (Fig. 7) with mass peaks at *m/z* 83.0, 85.0 and 87.0 corresponding to $CHCl_2^+$ as the dominant fragment [37]. After cooling, the sample retained crystallinity. The weight loss of 17.1% corresponded to the loss of approximately 2 $CHCl_3$ molecules per formula unit (calculated 18.6% from the molecular formula). In order to investigate whether the coordination network maintained its integrity, the same sample was placed in contact with $CHCl_3$ vapor for 48 h and was again analysed using TGA (Fig. S12). Loss of $CHCl_3$ was again detected confirming that, after the initial removal of solvent, the coordination assembly was able to re-absorb $CHCl_3$. A third cycle was performed with the same crystals exposed to $CDCl_3$ vapor for 24 h and then analysed by TGA (Fig. S13). Loss of $CDCl_3$ was confirmed by the presence of mass peaks at *m/z* 84.0, 86.0 and 88.0 corresponding to the $CDCl_2^+$ ion. In a fourth cycle, the crystalline material was recovered from the preceding TGA experiment and exposed to CH_2Cl_2 vapor for 24 h. The TGA trace of the resultant crystal showed loss of CH_2Cl_2 (*m/z* 49.0, 51.0, 84.0 and 86.0 arising from CH_2Cl^+ and $CH_2Cl_2^+$) at around 40 °C (Fig. S14). Finally, an analogous experiment was attempted using CCl_4 but the TGA of the crystals after exposure to CCl_4 vapor for 24 h revealed no change in mass over a period of 10 min heating at 80 °C. This is consistent with no uptake of CCl_4 into the crystal lattice.

$[Co(\mathbf{1})_2(NCS)_2]_n{\cdot}2nC_6H_5Me$ was also analysed by TGA. It was first heated to 150 °C and this temperature was maintained for 30 min. The loss of toluene was detected with peaks in the mass spectrum of the TGA-MS at *m/z* 92.0, 91.0 (highest intensity peak), 65.0 and 39.0 (Fig. 8). The weight loss of 14.4% (Fig. 8) corresponded to complete loss of two molecules of toluene from the lattice (calculated 15.0%). The same sample was then placed in contact with toluene vapor for 24 h, and the subsequent TGA analysis showed no appreciable mass loss, consistent with the fact that once toluene had been removed from $[Co(\mathbf{1})_2(NCS)_2]_n{\cdot}2nC_6H_5Me$, it was unable to be re-absorbed. This is consistent with the presence of the aromatic solvent in $[Co(\mathbf{1})_2(NCS)_2]_n{\cdot}2nC_6H_5Me$ playing a structural role in contrast to the $CHCl_3$ in $[Co(\mathbf{1})_2(NCS)_2]_n{\cdot}2nCHCl_3$ occupying channels in a non-ordered manner. The π-stacking interactions are key to the former, and we suggest that these may template the assembly of the network in $[Co(\mathbf{1})_2(NCS)_2]_n{\cdot}2nC_6H_5Me$ and that there is a partial loss in crystallinity (confirmed with PXRD) once the solvent is removed.

4. Conclusions

We have reported the synthesis and characterization of compound **1** which contains a 3,2′:6′,3″-tpy metal-binding domain. Under ambient conditions and using a solvent layering method, crystals of $[Co(\mathbf{1})_2(NCS)_2]_n{\cdot}2nCHCl_3$ and $[Co(\mathbf{1})_2(NCS)_2]_n{\cdot}2nC_6H_5Me$ were obtained.

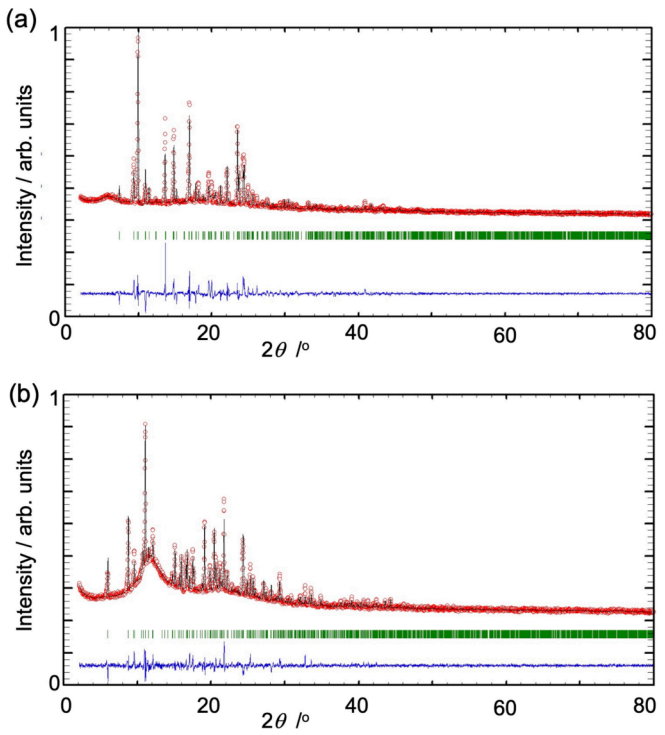

Fig. 6. PXRD (CuKα1 radiation) patterns (red circles) of the bulk crystalline materials of (a) $[Co(\mathbf{1})_2(NCS)_2]_n{\cdot}2n CHCl_3$, and (b) $[Co(\mathbf{1})_2(NCS)_2]_n{\cdot}2n C_6H_5Me$, with fitting to the predicted patterns from the single-crystal structures. The black lines are the best fits from the Rietveld refinements, and green lines show the Bragg peak positions. Each blue plot gives the difference between calculated and experimental points, and the differences in intensities arise from differences in the preferred orientations of the crystallites in the bulk samples.

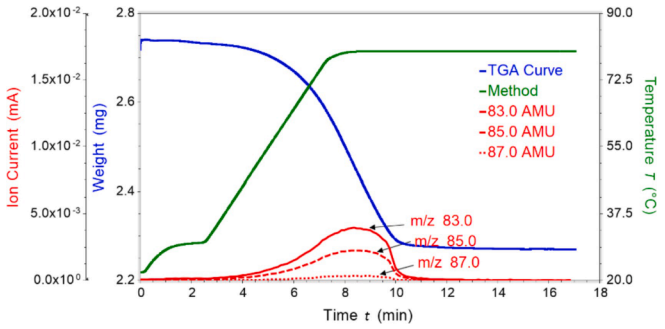

Fig. 7. TGA and mass spectrometric traces for the analysis of $[Co(\mathbf{1})_2(NCS)_2]_n{\cdot}2n CHCl_3$. Green: temperature vs. time; blue: weight of sample vs. time; red: mass detection for *m/z* 83.0 (most intense peak), 85.0 and 87.0. The initial mass of sample was 2.74 mg and a weight loss of 0.47 mg corresponds to 17.1%.

Single-crystal X-ray diffraction revealed that each is a 2D-coordination network with the Co atoms acting as 4-connecting nodes. In $[Co(\mathbf{1})_2(NCS)_2]_n{\cdot}2n CHCl_3$, the 3,2′:6′,3″-tpy unit in **1** adopts conformation **A** (Scheme 1) while conformation **B** is observed in $[Co(\mathbf{1})_2(NCS)_2]_n{\cdot}2n C_6H_5Me$. PXRD was used to confirm that the single crystals were representative of the bulk materials. In $[Co(\mathbf{1})_2(NCS)_2]_n{\cdot}2n CHCl_3$, ligands **1** are directed above and below the planar (4,4) net defined by the Co atoms. This leads to open channels running perpendicular to the nets. In $[Co(\mathbf{1})_2(NCS)_2]_n{\cdot}2n C_6H_5Me$ the toluene molecules, are involved in π-stacking interactions, and the solvent-accessible void-space comprises interlinked cavities. By using TGA-MS, we demonstrated that, after initial solvent loss from $[Co(\mathbf{1})_2(NCS)_2]_n{\cdot}2n CHCl_3$, $CHCl_3$, $CDCl_3$ or CH_2Cl_2 could be sequentially

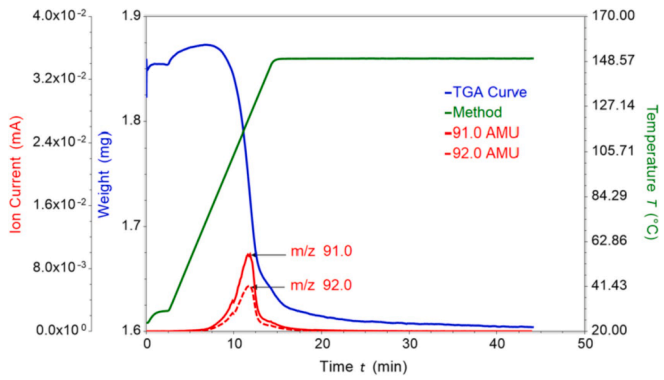

Fig. 8. TGA and mass spectrometric traces for the analysis of $[Co(\mathbf{1})_2(NCS)_2]_n{\cdot}2n C_6H_5Me$. Green: temperature vs. time; blue: weight of sample vs. time; red: mass detection for *m/z* 92.0, 91.0 (most intense peak), 65.0 and 39.0. The initial mass of sample was 1.87 mg and a weight loss of 0.27 mg corresponds to 14.4%.

introduced and removed from the same sample of single crystals. In stark contrast, the removal of toluene from $[Co(\mathbf{1})_2(NCS)_2]_n{\cdot}2n C_6H_5Me$ resulted in a partial loss in crystallinity (confirmed with PXRD), consistent with the aromatic solvent playing a role in stabilization of the structure.

Author Contributions

Experimental: D.R. and S.N.; Crystallography: A.P.; Powder diffraction and analysis: D.R.; Manuscript writing and structure analysis: D.R. and C.E.H.; Manuscript editing: all authors; Funding, project concepts and supervision: C.E.H. and E.C.C.

Declaration of Competing Interest

The authors declare that they have no known competing financial interests that could have appeared to influence the work reported in this paper.

Acknowledgements

We acknowledge financial support from the Swiss National Science Foundation (grant number 200020_182000) and the University of Basel. Sven Freimann (University of Basel) is thanked for his assistance with TGA measurements.

Appendix A. Supplementary data

Supplementary data (Figs. S1–S6: Mass spectrum, NMR spectra and IR spectrum of **1**. Figs. S7–S9: Additional crystallographic figures. Figs. S10 and S11: IR spectra of the coordination compounds. Figs. S12–S14: TGA-MS traces) to this article can be found online at https://doi.org/10.1016/j.poly.2021.115445.

References

[1] E.C. Constable, Adv. Inorg. Chem. 30 (1986) 69–121, https://doi.org/10.1016/S0898-8838(08)60240-8.
[2] E.C. Constable, Chem. Soc. Rev. 36 (2007) 246–253, https://doi.org/10.1039/B601166G.
[3] U.S. Schubert, H. Hofmeier, G.R. Newkome (Eds.), Modern Terpyridine Chemistry, Wiley, 2006.
[4] C. Wei, Y. He, X. Shi, Z. Song, Coord. Chem. Rev. 385 (2019) 1–19, https://doi.org/10.1016/j.ccr.2019.01.005.
[5] O.S. Taniya, D.S. Kopchuk, A.F. Khasanov, I.S. Kovalev, S. Santra, G.V. Zyryanov, A. Majee, V.N. Charushin, O.N. Chupakhin, Coord. Chem. Rev. 442 (2021), 213980, https://doi.org/10.1016/j.ccr.2021.213980.
[6] C.E. Housecroft, CrystEngComm 17 (2015) 7461–7468, https://doi.org/10.1039/C5CE01364J.

[7] C.E. Housecroft, E.C. Constable, Chem. Commun. 56 (2020) 10786–10794, https://doi.org/10.1039/d0cc04477f.
[8] S.M. Elahi, M. Raizada, P.K. Sahu, S. Konar, Chem. Eur. J. 27 (2021) 5858–5870, https://doi.org/10.1002/chem.202004651.
[9] C.E. Housecroft, E.C. Constable, Molecules 26 (2021) 3110, https://doi.org/10.3390/molecules26113110.
[10] D. Rocco, A. Prescimone, E.C. Constable, C.E. Housecroft, Molecules 25 (2020) 3162, https://doi.org/10.3390/molecules25143162.
[11] T.-T. Wang, J.-L. Zhang, H.-M. Hua, Y. Cheng, L.-L. Xue, X. Wanga, B.-Z. Wang, Polyhedron 151 (2018) 43–50, https://doi.org/10.1016/j.poly.2018.05.017.
[12] M. Zhao, J. Tan, J. Su, J. Zhang, S. Zhang, J. Wu, J. Tian, Dyes Pigm. 130 (2016) 216–225, https://doi.org/10.1016/j.dyepig.2016.03.005.
[13] D. Rocco, S. Novak, A. Prescimone, E.C. Constable, C.E. Housecroft, Chemistry 3 (2021) 182–198, https://doi.org/10.3390/chemistry3010015.
[14] Y.M. Klein, A. Lanzilotto, A. Prescimone, K.W. Kramer, S. Decurtins, S.-X. Liu, E. C. Constable, C.E. Housecroft, Polyhedron 129 (2017) 71–76, https://doi.org/10.1016/j.poly.2017.03.030.
[15] D. Rocco, A. Prescimone, Y.M. Klein, D.J. Gawryluk, E.C. Constable, C. E. Housecroft, Polymers 11 (2019) 1224, https://doi.org/10.3390/polym11071224.
[16] D. Rocco, A. Prescimone, E.C. Constable, C.E. Housecroft, Polymers 2020 (1823) 12, https://doi.org/10.3390/polym12081823.
[17] E.C. Constable, C.E. Housecroft, P. Kopecky, M. Neuburger, J.A. Zampese, G. Zhang, CrystEngComm. 14 (2012) 446–452, https://doi.org/10.1039/C1CE06024D.
[18] A.K. Mondal, S. Khatua, K. Tomar, S. Konar, Eur. J. Inorg. Chem. (2016) 3545–3552, https://doi.org/10.1002/ejic.201600569.
[19] Y.M. Klein, A. Prescimone, E.C. Constable, C.E. Housecroft, Materials 10 (2017) 728, https://doi.org/10.3390/ma10070728.
[20] Z. Yin, S. Zhang, S. Zheng, J.A. Golen, A.L. Rheingold, Polyhedron 101 (2015) 139–145, https://doi.org/10.1016/j.poly.2015.09.008.
[21] E.C. Constable, C.E. Housecroft, M. Neuburger, S. Vujovic, J.A. Zampese, G. Zhang, CrystEngComm. 14 (2012) 3554–3563, https://doi.org/10.1039/c2ce06609b.
[22] Y.M. Klein, A. Prescimone, E.C. Constable, C.E. Housecroft, Polyhedron 103A (2016) 58–65, https://doi.org/10.1016/j.poly.2015.08.005.
[23] Y.M. Klein, A. Prescimone, M.B. Pitak, S.J. Coles, E.C. Constable, C.E. Housecroft, CrystEngComm 18 (2016) 4704–4707, https://doi.org/10.1039/c6ce00939e.
[24] J. Granifo, M. Westermeyer, M. Riquelme, R. Gaviño, S. Suárez, E.B. Halac, R. Baggio, Acta Crystallogr. B 71 (2015) 805–813, https://doi.org/10.1107/S205252061501937X.
[25] E.C. Constable, C.E. Housecroft, S. Vujovic, J.A. Zampese, CrystEngComm 16 (2014) 328–338, https://doi.org/10.1039/C3CE42012D.
[26] Software for the Integration of CCD Detector System Bruker Analytical X-ray Systems; Bruker axs: Madison, WI, USA.
[27] G.M. Sheldrick, Acta Crystallogr. A 71 (2015) 3–8, https://doi.org/10.1107/S2053273314026370.
[28] O.V. Dolomanov, L.J. Bourhis, R.J. Gildea, J.A.K. Howard, H. Puschmann, J. Appl. Crystallogr. 42 (2009) 339–341, https://doi.org/10.1107/S0021889808042726.
[29] G.M. Sheldrick, Acta Crystallogr. C 27 (2015) 3–8, https://doi.org/10.1107/S002188980600731X.
[30] C.F. Macrae, I. Sovago, S.J. Cottrell, P.T.A. Galek, P. McCabe, E. Pidcock, M. Platings, G.P. Shields, J.S. Stevens, M. Towler, P.A. Wood, J. Appl. Crystallogr. 53 (2020) 226–235, https://doi.org/10.1107/S1600576719014092.
[31] A. LeBail, H. Duroy, J.L. Fourquet, Mat. Res. Bull. 23 (1988) 447–452, https://doi.org/10.1016/0025-5408(88)90019-0.
[32] G.S. Pawley, J. Appl. Crystallogr. 14 (1981) 357–361, https://doi.org/10.1107/S0021889881009618.
[33] J. Rodríguez-Carvajal, Physica B 192 (1993) 55–69, https://doi.org/10.1016/0921-4526(93)90108-I.
[34] T. Roisnel, J. Rodríguez-Carvajal, Proceedings of the Seventh European Powder Diffraction Conference (EPDIC 7) (2000) 118–123.
[35] J. Wang, G.S. Hanan, Synlett (2005) 1251–1254, https://doi.org/10.1080/00397910600616750.
[36] E.C. Constable, C.E. Housecroft, M. Neuburger, J. Schönle, S. Vujovic, J. A. Zampese, Polyhedron 62 (2013) 260–267, https://doi.org/10.1016/j.poly.2013.07.002.
[37] NIST Chemistry WebBook, http://webbook.nist.gov/chemistry, accessed 04.06.2021. doi:10.18434/T4D303.